MOLECULAR AND CELLULAR BIOLOGY, Aug. 2004, p. 7214–7224 Vol. 24, No. 16
0270-7306/04/$08.00+0 DOI: 10.1128/MCB.24.16.7214–7224.2004

Vanin-1$^{-/-}$ Mice Exhibit a Glutathione-Mediated Tissue Resistance to Oxidative Stress

C. Berruyer,[1]† F. M. Martin,[1]†‡ R. Castellano,[1] A. Macone,[2] F. Malergue,[1] S. Garrido-Urbani,[1] V. Millet,[1] J. Imbert,[3] S. Duprè,[2] G. Pitari,[4] P. Naquet,[1] and F. Galland[1]*

Centre d'Immunologie de Marseille-Luminy CNRS-INSERM-Université de la Méditerranée, 13288 Marseille,[1] and INSERM U599, 13009 Marseille,[3] France, and Dipartimento di Scienze Biochimiche "A. Rossi Fanelli," Instituto di Biologia e Patologia Molecolari del CNR, Università di Roma "La Sapienza," 00185 Rome[2] and Dipartimento di Biologia di Base ed Applicata, Università di L'Aquila, Coppito L'Aquila,[4] Italy

Received 6 January 2004/Returned for modification 9 February 2004/Accepted 6 May 2004

Vanin-1 is an epithelial ectoenzyme with pantetheinase activity and generating the amino-thiol cysteamine through the metabolism of pantothenic acid (vitamin B_5). Here we show that Vanin-1$^{-/-}$ mice, which lack cysteamine in tissues, exhibit resistance to oxidative injury induced by whole-body γ-irradiation or paraquat. This protection is correlated with reduced apoptosis and inflammation and is reversed by treating mutant animals with cystamine. The better tolerance of the Vanin-1$^{-/-}$ mice is associated with an enhanced gamma-glutamylcysteine synthetase activity in liver, probably due to the absence of cysteamine and leading to elevated stores of glutathione (GSH), the most potent cellular antioxidant. Consequently, Vanin-1$^{-/-}$ mice maintain a more reducing environment in tissue after exposure to irradiation. In normal mice, we found a stress-induced biphasic expression of Vanin-1 regulated via antioxidant response elements in its promoter region. This process should finely tune the redox environment and thus change an early inflammatory process into a late tissue repair process. We propose Vanin-1 as a key molecule to regulate the GSH-dependent response to oxidative injury in tissue at the epithelial level. Therefore, Vanin/pantetheinase inhibitors could be useful for treatment of damage due to irradiation and pro-oxidant inducers.

Oxidative stress is associated with the development and persistence of numerous physiopathological disorders. To date, an active area of investigation is focused on the cellular antioxidant network and the capacity of redox changes to trigger various biological events that include cell proliferation, differentiation, apoptosis, and inflammation. Glutathione (GSH) is considered to be the major thiol-disulfide redox buffer of the cell and tissues, and regulation of its metabolism has become a major therapeutic target in tissue repair.

Elimination of free radicals (i.e., reactive oxygen species [ROS]) and their toxic products occurs through the oxidation of GSH to glutathione disulfide (GSSG), subsequently regenerated by the glutathione reductase (GSH-Red). GSH homeostasis is also controlled by the gamma-glutamylcysteine synthetase (γGCS), the rate-limiting enzyme for GSH synthesis (17). The abundance of the γGCS mRNA is itself stress regulated via antioxidant response elements (AREs) found in the 5′-flanking region of the γGCS gene (21, 32, 47), and these AREs also regulate the coordinate induction of numerous oxidative stress response genes (36, 45).

Gamma irradiation disrupts water molecules, producing hydroxyl radicals and thus leading to oxidative damage and apoptosis in dividing cells. For example, the rapid renewal of the small intestine epithelium renders it highly sensitive to ionizing radiation, which provokes disruption of the mucosal integrity and progenitor crypt cell loss (42). The response of the intestinal epithelium to γ-irradiation is an established model to study the dynamics of epithelial cell regeneration after injury. Monitoring of γ-irradiation-induced thymic depletion is another classical strategy to assess the radiosensitivity of an animal. On whole-body irradiation, the thymus undergoes a drastic involution involving thymocyte death and stromal cell disorganization; it is fully reconstituted by bone marrow precursor cell injection (2). This "depletion-regeneration" model is convenient to study postirradiation tissue repair (43). We have chosen this approach to investigate the early events in interactions between thymocytes and thymic stromal cells and have identified Vanin-1, a cell surface molecule expressed by a subset of stromal cells, as being involved in postirradiation thymus reconstitution (3).

Vanin-1 is the prototypic member of a novel family of ectoenzymes including at least two proteins in mice (i.e., Vanin-1 and Vanin-3), three in humans (i.e., VNN1, VNN2, and VNN3), and *Drosophila* homologues (10, 11, 29). In mice, Vanin-1 and Vanin-3 expression is associated mostly with epithelial and myeloid cells, respectively (10, 11, 29). All Vanin molecules are pantetheinases (EC 3.5.1.-) capable of specifically hydrolyzing pantetheine into pantothenic acid (vitamin B_5) and cysteamine, a sulfhydryl compound used for antioxidant properties (9, 28, 34). The most important consequence observed in Vanin-1$^{-/-}$ mice is the lack of cysteamine in tissues where Vanin-1 expression is predominant, allowing us to probe the relative importance of this metabolite in the postirradiation tissue response (34).

* Corresponding author. Mailing address: Centre d'Immunologie de Marseille-Luminy CNRS-INSERM-Université de la Méditerranée, Parc scientifique de Luminy, case 906, cedex 9, 13288 Marseille, France. Phone: (33) 4 91 26 94 97. Fax: (33) 4 91 26 94 30. E-mail: galland@ciml.univ-mrs.fr.

† C.B. and F.M.M. contributed equally to this work.

‡ Present address: Department of Molecular and Experimental Medicine, The Scripps Research Institute, La Jolla, CA 92037.

We report here that Vanin-1$^{-/-}$ mice are more resistant to paraquat poisoning and exposure to lethal doses of γ-irradiation. Following irradiation, these mice display facilitated thymic reconstitution and a reduced apoptotic response in the small intestine, both of which are associated with a milder tissue inflammation. This protection is related to changes in the detoxifying potential of Vanin-1$^{-/-}$ tissues, characterized by elevated GSH stores. Importantly, intraperitoneal administration of cystamine (the disulfide form of cysteamine) abrogates the resistant phenotype of the mutant mice, suggesting that Vanin-1 regulates at least in part through cysteamine, the GSH-associated metabolism and modulates the adaptive tissue response to stress. On the other hand, Vanin gene expression is regulated during tissue reconstitution following γ-irradiation. The Vanin-1 gene promoter contains ARE-like elements involved in the enhanced expression of the gene on stress stimulation. We propose that Vanin/pantetheinase inhibitors could have useful applications in the therapy of damage due to radiation or other pro-oxidant inducers.

MATERIALS AND METHODS

In vitro experiments. The MTE-4-14 thymic epithelial cell line was subjected to γ-irradiation (5 or 20 Gy) or incubated with H_2O_2 (200 and 500 μM; Sigma) or 50 μM *tert*-butylhydroquinone (*t*-BHQ; Sigma) for various periods. For flow cytometric analysis of Vanin-1 expression, MTE-4-14 cells were stained with fluorescein isothiocyanate (FITC)-coupled monoclonal antibody (MAb) 407 (3) and analyzed on a FACSCalibur apparatus (BD Biosciences, Mountain View, Calif.).

In vivo experiments. Age-matched (3 to 4 months old) and weight-matched BALB/c control or Vanin-1$^{-/-}$ mice (at least nine generations of backcrosses) were kept in a specific-pathogen-free mouse facility and handled according to the rules of "Décret no. 87-848 du 19/10/1987, Paris." The mice were subjected to either sublethal (6-Gy) or lethal (10-Gy) doses of γ-irradiation, as indicated in the figure legends. For thymic regeneration, thymuses were removed on day 3 (short-term) and 8 (long-term) postirradiation and the cells were counted by trypan blue exclusion. For short-term experiments, bone marrow cells were labeled for 7 min at 37°C with 10 μM CFDA-SE (Molecular Probes) at 10^7 cells per ml in phosphate-buffered saline (PBS) (Invitrogen). Labeled cells (3×10^7) were injected intravenously into each irradiated recipient mouse. Cytofluorimetric analysis was performed on a fluorescence-activated cell sorter analyzer (Beckton Dickinson). For intestinal experiments, the ileum was removed 4 or 10 h postirradiation and apoptotic cells were detected on 5-μm fixed tissue sections by using annexin V (FITC-labeled annexin V kit; Euromedex) or terminal deoxynucleotidyl transferase-mediated dUTP-biotin nick end labeling (TUNEL) staining (in situ cell death detection kit, TMR red; Roche). For paraquat toxicity, mice were injected intraperitonealy with 70 μg/g of body weight. Intraperitoneal injections of cystamine (120 mg/kg of body weight) were started 2 days before exposure to stress (paraquat or γ-irradiation) and were repeated daily for the duration of the various in vivo assays.

Immunohistological analysis. Tissues were embedded in Tissue-Tek OCT compound (Sakura) and frozen. Acetone-fixed 8-μm-thick cryosections were stained with MAb 407 and revealed with a mouse-adsorbed goat anti-rat immunoglobulin-horseradish peroxidate complex (Southern Biotechnology associates, Birmingham, Ala.) and tyramide signal amplification (TSA cyanine 3 system; Perkin-Elmer Life Sciences). After saturation with 10% normal rat serum (TEBU CALTAG Laboratories), double staining was performed using the FITC-coupled anti-EpCAM MAb (29 antigen [33]) (and isotypic negative controls) diluted in 5% normal rat serum blocking buffer. Microscopy analysis was performed using an Axiovert microscope coupled to an Axiocam MRC camera (Zeiss).

Sorting of thymic cell populations. Stromal and lymphoid thymic cell populations were sorted from dissociated thymuses by using a FACStar-Plus apparatus (Becton Dickinson) and FITC- or phycoerythrin-conjugated antibodies directed against EpCAM, CD11c, CD4, and CD8 (Pharmigen).

RT-PCR and TaqMan-PCR experiments. Total RNAs were isolated using the TRIzol Reagent (Invitrogen). RNA (1 μg) was reverse transcribed with oligo(dT), using the Stratascript enzyme (Stratagene). The relative amounts of cDNAs produced were estimated by amplification of actin or glyceraldehyde-3-phosphate dehydrogerase cDNAs during different cycles, in order to use standardized amounts of cDNA in the PCR (*Taq* polymerase [Invitrogen]). PCR products were run on agarose gels, and the gels were scanned with a digital charge-coupled device video camera. Quantitative evaluation of the PCR products was done using the Advanced Image Data Analyzer (Aida 1000/1D software 1.01; Raytest GmbH). This analysis was performed on three animals for each condition. The markers tested were interleukin-1β (IL-1β), IL6, tumor necrosis factor alpha, gamma interferon inducible nitric oxide synthese (iNOS), COX1, COX2, and MIP2; only results with $P < 0.05$ between wild-type WT and Vanin-1$^{-/-}$ samples are shown.

Real-time quantitative reverse transcription PCR (RT-PCR) (TaqMan PCR) was performed with the ABI PRISM 7700 sequence detection system (Perkin-Elmer) using SYBR green for product measurement. Each primer set gave a unique product (actin, 5′-CATCCTGGCCTCGCTGTC-3′ and 5′-CTCGTCGTACTCCTGCTTGGT-3′; Vanin-1, 5′-GGAACCCGGTATGTCTTCCC-3′ and 5′-ACTCCCCAGGTGCGAGC-3′; Vanin-3, 5′-ACAAGATGTCTGAAAGCCGAATG-3′ and 5′-TGTATGGAGTCCATCAAAGGCA-3′; MT-1, 5′-TGCTCCACCGGCGG-3′ and 5′-TTTGCAGACACAGCCCTGG-3′). Values were determined by reference to a standard curve generated by a serial dilution of cDNA and normalized by the levels of actin mRNA. Threshold cycle (C_T) determinations were automatically performed by the instrument for each reaction (18). A variation of one cycle was evaluated to a twofold increase in gene expression, using various dilutions of actin template as control.

Northern blot and dot blot RNA. For Northern blot analysis, 20 μg of total liver and kidney RNA was run on formaldehyde denaturing agarose gels and transferred to a nylon membrane (Appligene). For dot blot RNA, 2 μg of total RNA was denaturated (50% deionized formamide) and spotted onto a nylon membrane. Hybridizations were performed in Express Hyb solution (Clontech) with ^{32}P-labeled DNA probes corresponding to PCR fragments obtained using the following primer sets: actin, 5′-GTGGGCCGCTCTAGGCACCAA-3′ and 5′-CTCTTTGATGTCACGCACGATTTC-3′; Vanin-1, 5′-CGGTGCAGGAGAGACTCAGC-3′ and 5′-GCCAAATGAGGAAGGACGTC-3′; Vanin-3, 5′-CAGTACAGGAGAGACTGAGC-3′ and 5′-TCACCAGCTCTGAATCTTTG-3′; and MT-1, 5′-CTTCACCAGATCTCGGAATGG-3′ and 5′-ACATCAGGCACAGCACGTGC-3′. The membranes were exposed for autoradiography with FUJI screen (FUJI BAS 1000) or Kodak film. Quantifications (dot blot or Northern blot) were done using a TINAbas reader and phosphorimager (FUJI BAS 1000). Each band and each spot were normalized by the actin signal (intensity of observed spot/intensity of actin spot).

Transient transfections and reporter gene assays. Mouse Vanin promoters were obtained by PCR using the Herculase high-fidelity polymerase (Stratagene) starting with phage λ GV3 or cosmid A5 clones as template DNAs for Vanin-1 and Vanin-3, respectively (29). PCR products were cloned into the pGEM-TEasy vector (Promega) and subcloned into the promoterless pGL3-Basic luciferase reporter vector (Promega). The pV1-*s* clone contains a "short promoter" (±1 kb) with the proximal Vanin-1 ARE-L1 site. The pV1-*l* clone contains a "long promoter" (± 3.5 kb) with the two Vanin-1 ARE sites (ARE-L1 + ARE-L2) (see Fig. 5C). Inactivating mutations in the core region of ARE sites (TGAC to AAAC) were performed using the QuickChange site-directed mutagenesis kit (Stratagene). Luciferase reporter constructs were checked by sequencing (DNA sequence kit, BigDyeTMTerminator cycle sequencing [PE-Applied Biosystems], ABI PRISM 310 [Perkin-Elmer]) and then transfected into the MTE-4-14 cell line with the Fugene 6 transfection reagent (Roche). A 1-μg sample of each reporter construct was cotransfected with 0.1 μg of *Renilla* pTK. At 36 h later, 50 μM *t*-BHQ was added. The cells were harvested after 48 h and firefly and *Renilla* luciferase activities were measured (dual luciferase reporter gene assay kit; Promega). Reporter activity was calculated as the ratio of firefly luciferase activity to *Renilla* luciferase activity. Transfections were done in duplicate and repeated three times.

Electrophoretic mobility shift assay (EMSA). Preparation of MTE-4-14 nuclear extracts, end labeling of the probe, binding reaction, and polyacrylamide gel analysis were performed as previously described (6). The following double strands oligonucleotides were used in this study: ARE-L1, 5′-GGAACCACGTGACTCATGCCTTGTTTATA-3′; ARE-L2, 5′-TCAGGAGGAGTGACCGTGGCTACAACCATG-3′; ARE-L1mut, 5′-GGAACCACGAAACTCATGCCTTGTTTATA-3′; ARE-L2mut, 5′-TCAGGAGGAGAAAACCGTGGCTACAACCATG-3′; MT-1, 5′-GATCCGCGGGGCGCGTGACTATGCGTGGGCTGGA-3′; SP1, 5′-CCAGGGAGGCGTGGCCTGGGCGGGACTGGGGAGTGGCGAGCC-3′; and AP1, 5′-CTAGTGATGAGTCAGCCGGATC-3′. Supershift and competition assays were performed by incubating the reaction mixtures for 20 min with the antisera or a 100-fold excess of cold competitor before addition of the labeled probe. The following rabbit polyclonal antisera were used: anti-

SP1 (Euromedex, no. 07-124), anti-Jun B (Santa Cruz, no. SC-48), anti-cFos (no. SC-253), and anti-ATF1 (no. SC-270).

Determination of enzyme activities on tissues. Tissue homogenates were obtained by using Ultraturax in 10 mM phosphate buffer (pH 7.0) (1:5, wt/vol) containing 1 mM dithiothreitol, and γGCS activity was measured on the basis of ATP formation by using a pyruvate kinase-lactate dehydrogenase coupling assay (40). Oxidation of NADH was spectrophotometrically monitored and assumed to equal the rate of ADP formation. One unit was defined as the amount of enzyme producing 1 μmol of ADP/min. The oxidation of NADPH in a GSSG reductase-coupled assay was measured for the determination of specific activity: 1 unit was defined as the amount of GSH oxidized per minute. GSH reductase was measured as described previously (8). One unit was defined as the amount needed to oxidize 1 μmol of NADPH/min. GSH transferase activity toward 1-chloro-2,4-dinitrobenzene was assayed as described previously (13).

GSH determination. Determination of GSH and GSSG was performed on 5% trichloroacetic acid homogenates (1:5, wt/vol). After centrifugation, samples were diluted 1:10 with running buffer, filtered through a Microcon YM-10 centrifugal filter device (Amicon), and analyzed after high-performance liquid chromatography separation and electrochemical detection with a four-channel coulometric sensor (ESA model 6210) performed at 700, 800, 900 and 1,000 mV. A Nova Pack C_8 column (pore size, 4 μm; 4.6 by 250 mm [Waters]) was used, and the isocratic run was at 1 ml/min with 50 mM phosphate buffer (pH 3.0). Linear standard curves were obtained with both reduced (run time, about 3.5 min) and oxidized (run time about 4.3 min) GSH. Internal standards were added for identification; detection limits were about 50 pmol for GSH and 100 pmol for GSSG.

Exploration of ROS and protein oxidation. To measure ROS, red blood cells were incubated with 10 μM 2′,7′-dichlorodihydrofluorescein diacetate (DCF; Sigma) for 15 min at 37°C and then the intracellular fluorescence intensity was analyzed by flow cytometry. Immunoblot detection of carbonyl groups introduced into proteins by oxidative reaction was carried out using the OxyBlot protein oxidation kit (Chemicon) as specified by the manufacturer, starting with liver lysates from four animals for each condition (20 mg of protein was used for sodium dodecyl sulfate-polyacrylamide gel electrophoresis).

Statistical analysis. Data are expressed as mean ± standard deviation. Values from experimental and control groups were compared using Student's t test. Probability values of $P < 0.05$ were considered statistically significant.

RESULTS

Lack of Vanin-1 leads to improved thymic reconstitution following irradiation. Based on antibody-blocking experiments, the initial description of Vanin-1 suggested a role in thymus homing (3). As expected, anti-Vanin-1 MAb subclones (407.6.3 and 407.7.4) inhibited thymic regeneration in WT but, importantly, not in Vanin-$1^{-/-}$ mice in in vivo reconstitution experiments following irradiation (Fig. 1A). In addition, Vanin-$1^{-/-}$ mice showed an accelerated reconstitution following irradiation (Fig. 1B). Similar assays were performed with intravenous injection of labeled bone marrow cells (CFDA-SE), and on day 3, a mean increase of 49% in the number of CFDA-SE^+ cells was detected in Vanin-$1^{-/-}$ thymuses (Fig. 1B). In conclusion, Vanin-$1^{-/-}$ mice display an improved thymic reconstitution that could be due, at least partially, to the enhanced entry of new bone marrow-derived cells. This phenotype is the opposite of that observed with the anti-Vanin-1 antibodies. In vitro, anti-Vanin-1 MAb 407 does not inhibit the enzymatic activity of Vanin-1 on transfected cells (data not shown), suggesting that this antibody could not mimic the knockout phenotype by pantetheinase inhibition; its mechanism of action is unknown at present.

Vanin gene expression is up-regulated by oxidative stress. We first described Vanin-1 as a molecule weakly expressed by some epithelial and perivascular thymic cells (3). The availability of both an enhanced detection technique (see Materials and Methods) and control Vanin-$1^{-/-}$ animals allowed a better definition of Vanin-1^+ cells in thymus. As shown on thymic sections, the Vanin-1-specific MAb 407.7.4 stains few Ep-CAM^+ thymic medullary epithelial (Fig. 2A) but not the 735^+ perivascular cells (not shown). This finding was proven by the absence of staining in Vanin-$1^{-/-}$ mice (Fig. 2A) as well as $RelB^{-/-}$ thymuses, which lack $EpCAM^+$ cells (reference 33 and data not shown) and confirmed by RT-PCR analysis of thymic sorted cells (Fig. 2B). Furthermore, RT-PCR revealed the coexpression of the Vanin-1 and Vanin-3 transcripts by the $EpCAM^+$ CD11c-epithelial cell subset.

We next explored the kinetics of Vanin-1 and Vanin-3 thymic expression following irradiation (6 Gy) (Fig. 2C and D). In all cases, ionizing radiation provoked a transient increase in

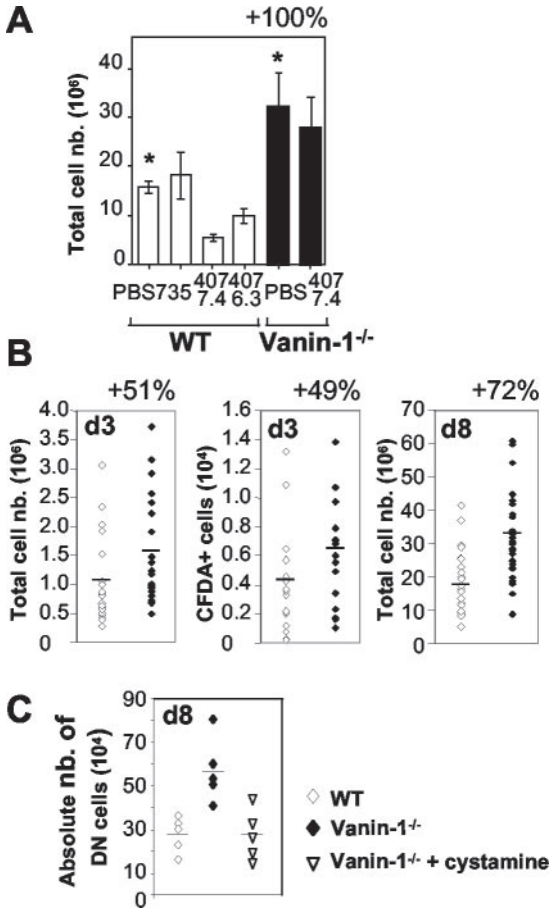

FIG. 1. Improved regeneration of irradiated thymus in Vanin-$1^{-/-}$ mice. Thymic reconstitution in whole-body-irradiated mice (6 Gy) was estimated by the total cell count. (A) Anti-Vanin-1 (407-7-4 and 407-6-3) or isotype-matched control (735) antibodies (50 μg) were injected intravenously into WT or Vanin-$1^{-/-}$ mice ($n = 5$). PBS was used as a control. White bars show WT mice, and black bars show Vanin-$1^{-/-}$ mice. *, $P < 0.001$. (B) Thymic cellularity in WT and Vanin-$1^{-/-}$ mice on day 3 (d3; $n = 22$ and 24, respectively; $P < 0.02$) or day 8 (d8; $n = 29$ and 31, respectively; $P < 0.0001$) postirradiation. Where indicated, some irradiated mice received 3×10^7 CFDA-SE-labeled bone marrow cells intravenously, and intrathymic fluorescence-positive cells were counted by cytofluorimetry on day 3 ($n = 15$ and 17, respectively; $P < 0.05$). (C) Counting of the immature DN $CD4^-$ $CD8^-$ T cells in thymus 8 days after irradiation. For statistical analysis, $P < 0.005$ comparing WT with Vanin-$1^{-/-}$ mice and nontreated with treated Vanin-$1^{-/-}$ mice. Each point is representative of an animal.

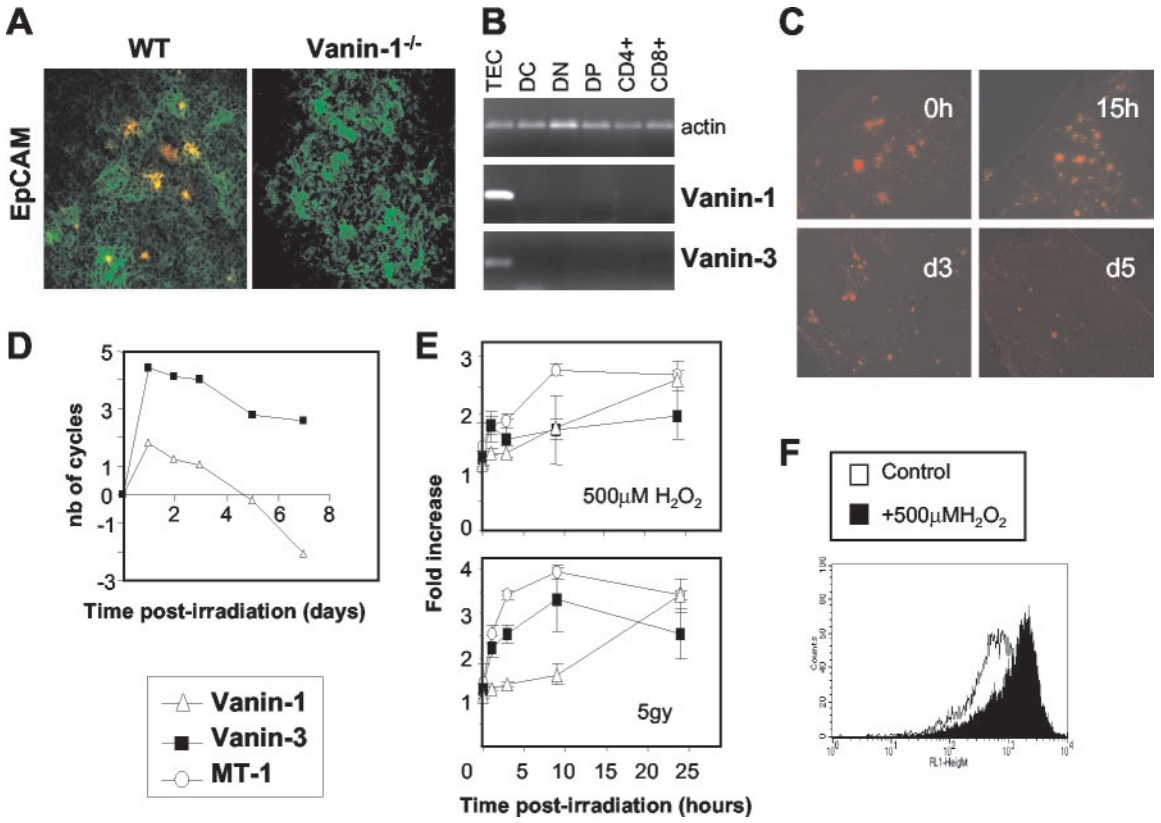

FIG. 2. Vanin gene expression in the thymus is restricted to the EpCAM$^+$ epithelial cells and regulated following irradiation. (A) Double staining of thymic sections from WT and Vanin-1$^{-/-}$ mice, using the anti-Vanin-1 407 MAb, revealed by tyramide staining (red) and the FITC-coupled EpCAM MAb (green). (B) RT-PCR analysis of the distribution of the Vanin-1 and Vanin-3 transcripts in thymic sorted cell populations. (C) Kinetic analysis of Vanin-1 expression in irradiated thymuses by immunohistology using MAb 407 revealed by tyramide staining (red). (D) Real-time RT-PCR determination of the Vanin-1 and Vanin-3 transcripts in the thymus postirradiation. Values represent the difference in the number of cycles between each time point and the physiological conditions fixed to 0 (a variation of one cycle was equivalent to a two-fold increase in gene expression). (E) RNA dot blot results showing up-regulation of the Vanin-1 and Vanin-3 mRNAs in cultured TECs subjected to 500 μM H_2O_2 or 5 Gy of γ-irradiation. Expression of the MT-1 gene was monitored as a stress-inducible positive control. Data represent the combined result of three independent experiments. (F) Flow cytometric detection of the cell surface expression of the Vanin-1 protein (MAb 407) by TECs with or without incubated with 500 μM H_2O_2 for 12 h.

Vanin gene expression for the first 2 days postirradiation. Gamma irradiation depletes the lymphoid compartment, which is predominant in cell number; therefore, we normalized the PCR results by using the amplification of keratin 14, a thymic medullary epithelium marker (reference 22 and data not shown). After correction, the results documented a two- to four-fold increase and a sixfold increase of Vanin-1 and Vanin-3 expression, respectively, followed by down-regulation leading to undetectable levels after day 3 for Vanin-1.

We then examined the in vitro effect of γ-irradiation (5 Gy) or H_2O_2 (500 μM), as another stress stimulus, on a thymic epithelial cell line (TEC) and showed that both stimuli led to a 2.5- to 3.4-fold increase in the levels of Vanin-1 mRNA and protein (Fig. 2E and F). For Vanin-3, the maximal induction was observed earlier (1.9- to 3.3-fold at 1 h postirradiation and after 10 h of H_2O_2 treatment, respectively).

A two- to threefold induction of Vanin mRNA was also detected in tissues by three independent assays; RNA dot blots (data not shown), Northern blots (Fig. 3A) and real-time quantitative PCR (Fig. 3B) documented that the level was induced two-to threefold by irradiation. In all these experiments, the expression of the metallothionein-1 gene (MT-1) was monitored as a positive control of stress-induced transcriptional response (1). Thus, transcription of the Vanin genes is regulated by oxidative stress. Interestingly, we noticed a higher expression of Vanin-3 in Vanin-1$^{-/-}$ tissues.

The Vanin-1 promoter contains functional ARE-like elements. We cloned the 5′-flanking region of the Vanin-1 gene and two TGACNNNNGC ARE-like elements (ARE-L) containing four N nucleotides instead of three in the TGAC NNNGC ARE consensus core motif were identified at positions −67 (ARE-L1 = TGACTCATGC) and −2016 (ARE-L2 = TGACCGTGGC) relative to the ATG initiator site (fig. 4A). Experiments were performed to determine whether these motifs functioned as stress-regulated targets within the Vanin-1 promoter by generating luciferase reporter constructs displaying one (e.g., pV1-*s*) or two (e.g., pV1-*l*) ARE-like elements. TECs were transfected with the different constructs and exposed to *t*-BHQ, the prototypic inducer of ARE-drive transcription (4). As shown in Fig. 4B, the luciferase activities of pV1-*s* and pV1-*l* were 1.5- to 2-fold greater after *t*-BHQ treatment (50 μM) than in the absence of this compound.

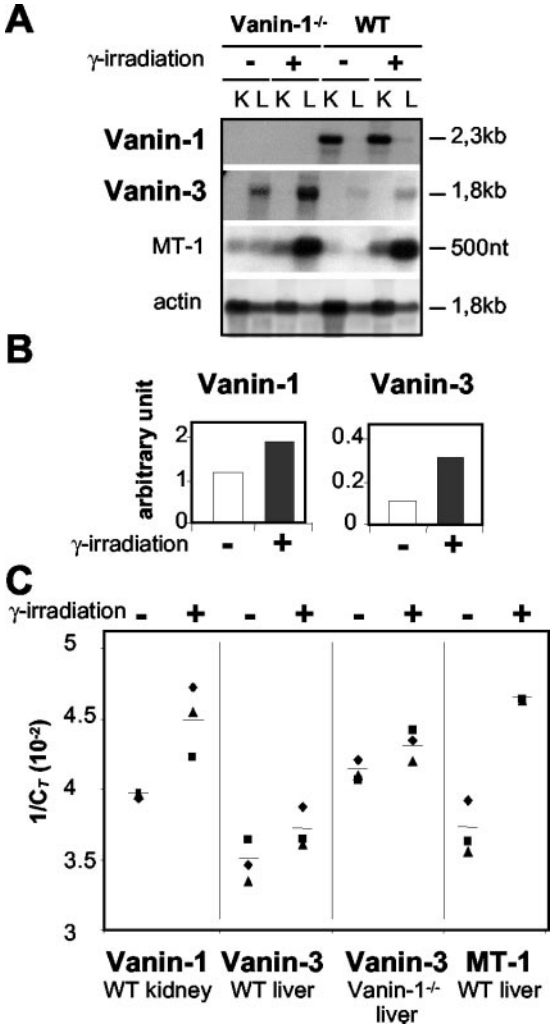

FIG. 3. In vivo up-regulation of Vanin gene expression following whole-body irradiation. (A and B) Analysis of Vanin-1 and Vanin-3 expression in kidney (K) or liver (L) from WT or Vanin-$1^{-/-}$ mice subjected to γ-irradiation (6 Gy) or not irradiated. MT-1 and actin were assayed simultaneously as postive and negative controls, respectively. Studies were performed by Northern blot analysis 9 h postirradiation (A), and results were quantified using the TINAbas reader and phosphorimager (FUJI BAS 1000) (B). (C) Real-time RT-PCR was used and values are shown as $1/C_T$, where C_T represents the threshold cycle. A high C_T value corresponds to a small amount of template DNA, and a low C_T value corresponds to a large amount of template present initially (18). Each point represents independent experiments with on different animals.

Furthermore, the basal luciferase activity of pV1-*l*, which contains ARE-L1 plus ARE-L2 was double that of pV1-*s*, containing only ARE-L1. This supported a role of the Vanin-1 ARE-like sequences as bona fide AREs. To test this hypothesis, we used pV1-*s*Mut and pV1-*l*Mut reporter constructs containing mutations in the core TGAC (AAACNNNNGC) of the ARE-L1 or ARE-L2 site, respectively. Induction of luciferase activity by *t*-BHQ was lost in pV1-*s*Mut, but the constitutive expression was also abolished (Fig. 4B). Surprisingly, the activity of pV1-*l*Mut containing a normal ARE-L1 and a mutated ARE-L2 was greater than that of the normal pV1-*l* itself and did not respond to the *t*-BHQ induction, suggesting that the mutation in the ARE-L2 site abolished an unexpected negative regulatory process. Similar results were obtained after incubation with H_2O_2 (data not shown) and led us to conclude that the ARE-like elements of Vanin-1 control the basal and stress-regulated response of the Vanin-1 gene.

EMSA was used to detect the ARE-L1 and ARE-L2 binding activity in nuclear extracts from TECs (Fig. 4). The previously described ARE site from the MT-1 gene promoter was used as a positive control of the stress-induced DNA binding site (7). Consistent with the luciferase reporter studies, EMSA showed protein-DNA complexes already formed with ARE-L1 and ARE-L2 sequences by using extracts derived from cells in the absence of stress-inducing compound conditions. However, as expected, a moderate increase in the complexes formed was observed after H_2O_2 or *t*-BHQ treatment (Fig. 4A). These complexes were undetectable when the mutated ARE-L1 and ARE-L2 sequences were used as target oligonucleotides (Fig. 4C). By competition assays, we first verified the specificity of these complexes and demonstrated that they were almost completely abolished by addition of unlabeled ARE-L1 or ARE-L2 oligonucleotides but not by a similar molar excess of corresponding mutant AREs (fig. 4D and E). We further tried to identify the nature of the nuclear factors involved and showed that AP-1 and SP-1 binding sites but not ATF1 (or Nrf2, NF-κB, or GSTα2–ARE-L2 [data not shown]) competed for complex formation with ARE-L1 and ARE-L2, respectively. Finally, supershift experiments were carried out using a set of specific antibodies to the nuclear extracts before EMSA. Figure 4D shows a reproducible decrease in the number of ARE-L1-specific protein-DNA binding complexes as well as a retarded mobility when anti-JunB or c-Fos antibodies were added. This suggests occupancy of the ARE-L1 site by an AP-1-like complex composed mainly of c-Fos and, to a lesser extent, JunB (Fig. 4D). However, in competition assays, some ARE-L1 complexes still remained visible in excess of AP-1-specific double-stranded oligonucleotides, suggesting that binding of other polypeptides might be involved. Similarly, supershift assay with an anti-SP-1 antibody showed a strong diminution in the amount of the DNA-protein complex formed with the ARE-L2 sequence (fig. 4E). Thus, both ARE-like binding sites of the Vanin-1 gene promoter are specifically occupied in vitro by nuclear factors, including at least AP-1 and SP-1 for ARE-L1 and ARE-L2, respectively, and these protein-DNA complexes are slightly enhanced under stress conditions.

Vanin-$1^{-/-}$ mice display reduced apoptotic and inflammatory responses to irradiation. Ionizing irradiation induces the generation of ROS in tissues and provokes the accumulation of phagocytes, which cause additional release of ROS and cytokines involved in the physiopathology of radiation injury. Using tyramide staining as a substrate for the endogenous tissue peroxidase, we detected less activated phagocytes in thymuses of Vanin-$1^{-/-}$ compared to WT control animals 24 h postirradiation (Fig. 5A). Vanin-1 is highly expressed by the intestinal mucosa (30), which is a critical target for radiation induced damage. Therefore, using both postirradiation models of thymus and intestinal regeneration, we estimated the amounts of inflammatory markers by RT-PCR. Significantly lower levels of transcripts encoding proinflammatory cytokines (IL-1β and IL-6), neutrophil chemoattractant (MIP-2), and oxidative marker

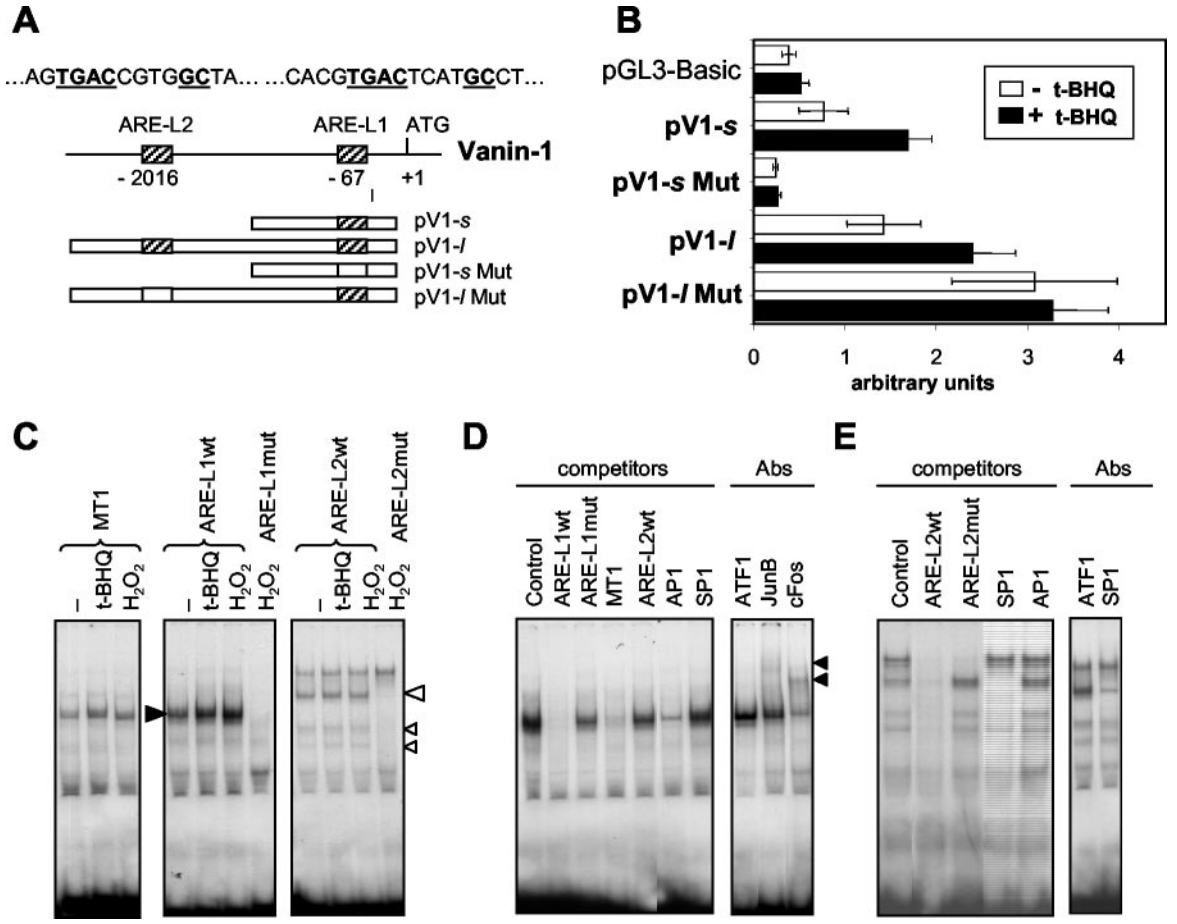

FIG. 4. Involvement of AREs in the stress-induced modulation of Vanin-1 expression. (A) Diagram of the 5′-flanking region of the Vanin-1 gene (arbitrary scale), together with the different pGL3-Basic luciferase reporter constructs containing one or two normal (hatched boxes) or mutated (white boxes) ARE-like elements. (B) Luciferase reporter gene assays were performed with TECs transiently transfected (48 h) with the pGL3-Basic vector control or various Vanin-1 promoter constructs and subjected to 50 μM *t*-BHQ for 12 h or left untreated. (C to E) Characterization of the factors binding to ARE-L1 and ARE-L2 sequences. ^{32}P-labeled WT or mutated (Mut) ARE-L1 and ARE-L2 probes or a MT-1 promoter-derived ARE probe were incubated with nuclear extracts (5 μg) prepared from unstimulated (−), *t*-BHQ-stimulated (1 h, 50 μM), or H_2O_2-stimulated (1 h, 500 μM) TECs. The position of the major complexes observed with the WT ARE-L1 and ARE-L2 probes are indicated by solid and open arrowheads, respectively. Competition studies showed in panels D and E for ARE-L1 and ARE-L2, respectively, were carried out by adding a 100-fold excess of an unlabeled WT or Mut ARE-L1, WT ARE-L2, MT-1, AP-1, or SP-1 oligonucleotide to the nuclear extract from H_2O_2-treated cells. When indicated, the binding-reaction mixture also contained a specific antibody directed against ATF1, cFos, Jun B, or SP-1 protein, and arrows identify specific retarded complexes.

for activated neutrophils (iNOS) were observed in the thymuses of Vanin-1$^{-/-}$ compared to WT mice (Fig. 5B). A similar result was observed in the ilea of Vanin-1$^{-/-}$ mice, with less detectable MIP-2, iNOS, and COX2, the inducible enzyme involved in the synthesis of prostaglandins (Fig. 5C). Thus, Vanin-1$^{-/-}$ tissues displayed a weaker inflammatory-type response after irradiation.

Ionizing radiation triggers cellular apoptotic responses within the small intestine. Frozen sections of ileum were obtained from WT and Vanin-1$^{-/-}$ mice 4 or 10 h after exposure to whole-body irradiation (10 Gy). In all cases, a combined analysis of exposed phosphatidylserine on the outer leaflet of the cell membrane by annexin V and DNA fragmentation by TUNEL indicated a lower frequency of apoptotic cells in the lamina propria of the small intestines of Vanin-1$^{-/-}$ versus WT mice (Fig. 5D to F).

Increased resistance of Vanin-1$^{-/-}$ mice to systemic oxidative stress. Since Vanin genes responded to various stress inducers and Vanin-1$^{-/-}$ mice displayed facilitated thymus recovery after irradiation, we examined the survival of mice exposed to oxidative damage by poisoning with paraquat, a redox-cycling bipyridyl herbicide (16), or by a lethal dose of γ-irradiation (10 Gy). As shown in Fig. 6A, 50% of WT controls died during the first 40 h after paraquat injection whereas 90% of the Vanin-1$^{-/-}$ mice remained alive. Similarly (Fig. 6C), 50% of WT control mice were dead on day 7 and 100% were dead day 10 postirradiation. In contrast, the median survival time observed for the Vanin-1$^{-/-}$ mice was 12 days ($P < 0.04$), and 10% of the mice were still alive 13 days postirradiation.

Administration of cystamine reverses the mutant phenotype of Vanin-1$^{-/-}$ mice. Cysteamine is specifically produced by

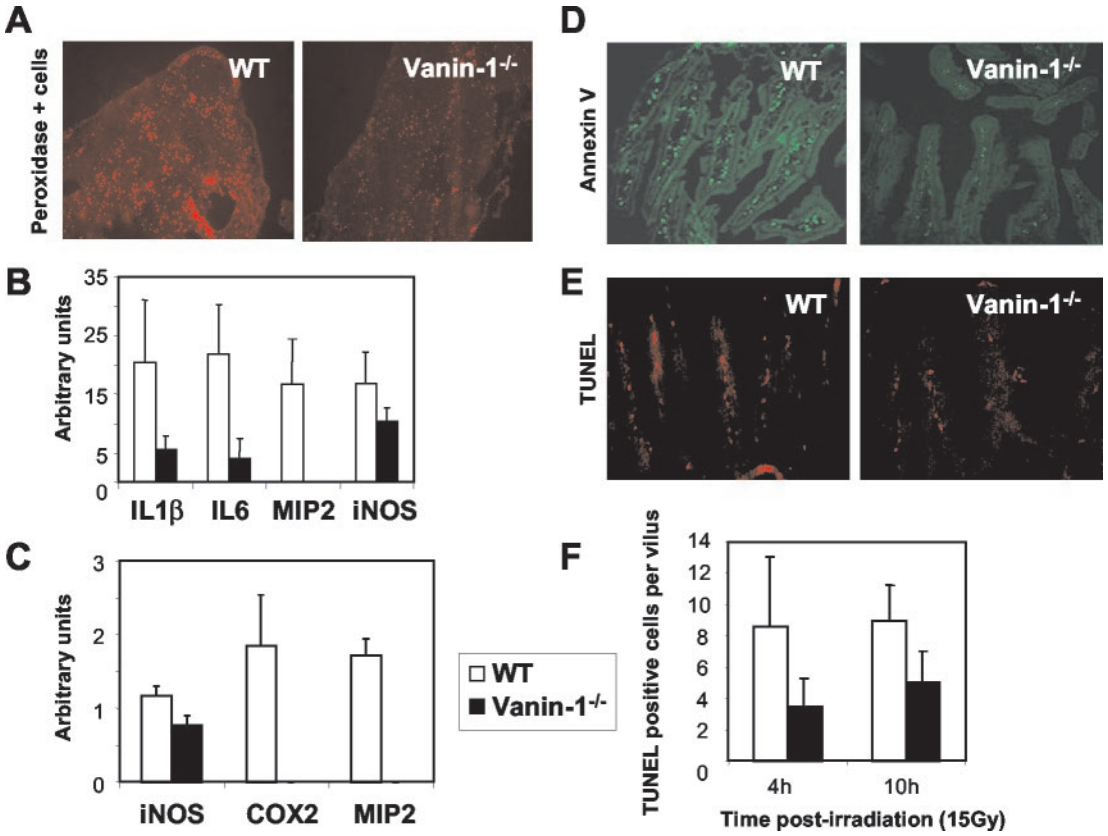

FIG. 5. Moderate inflammation and reduced apoptosis in tissues of Vanin-1$^{-/-}$ mice following irradiation. (A) Tyramide staining reveal the endogenous peroxidase activity was done on thymic cryosections from WT and Vanin-1$^{-/-}$ mice 24 h postirradiation (6 Gy). (B and C) Quantification of the RT-PCR detection of transcripts encoding proinflammatory markers in WT and Vanin-1$^{-/-}$ thymus (B) or ileum (C) 24 h postirradiation (6 Gy). This analysis was performed with three animals for each condition. Only results with $P < 0.05$ are shown. (D and E) Histological revealation of FITC-labeled annexin V-positive (green) or TUNEL-positive (red) apoptotic cells within the ileum 10 h after irradiation (10 Gy). (F) Quantification of TUNEL-positive cells per villus observed postirradiation (10 Gy). Samples were removed at 4 h (WT $n = 10$, Vanin-1$^{-/-}$ $n = 5$; $P < 0.03$) and 10 h (WT $n = 4$, Vanin-1$^{-/-}$ n = 3; $P < 0.04$).

pantheteinase activity. To estimate its contribution in the protected phenotype of Vanin-1$^{-/-}$ mice, we injected cystamine intraperitoneally into cohorts of animals daily in the various in vivo assays. In all models, cystamine administration completely reversed the mutant phenotype. In thymic reconstitution assays, the number of the most immature thymocytes (double-negative CD4$^-$ CD8$^-$ [DN] T cells) 8 days postirradiation was comparable between cystamine-treated Vanin-1$^{-/-}$ and WT mice (Fig. 1C). Similarly, cystamine-treated Vanin-1$^{-/-}$ mice had a reduced survival after exposure to a lethal dose of γ-irradiation or paraquat injection (Fig. 6A to C).

Increased γGCS activity and GSH levels in liver are related to the Vanin-1$^{-/-}$ protection to radiation. The liver is the most important organ for GSH synthesis, and although both Vanin-1 and Vanin-3 are expressed in this organ, Vanin-1$^{-/-}$ mice lack free cysteamine in the liver (34). In this study, we showed that Vanin-1$^{-/-}$ mice are protected from oxidative stress and that cysteamine administration to these animals repressed this protection. It has been reported that cysteamine inhibits the γGCS activity in vitro (12, 23). Here we report that Vanin-1$^{-/-}$ mice have a significantly higher γGCS activity in the liver: 53.3 ± 3 and 32 ± 2.7 mU/mg of protein ($n = 5$), for Vanin-1$^{-/-}$ and WT mice, respectively. As expected, this difference in γGCS activity was correlated with higher liver GSH store (10.09 ± 3.84 and 5.35 ± 1.05 μmol/mg of protein, [$n = 6$] for Vanin-1$^{-/-}$ and WT mice, respectively), as well as lower levels of oxidized GSSG (0.48 ± 0.18 and 0.62 ± 0.34 μmol/mg of protein [$n = 6$], respectively), whereas recycling by GSH-Red did not appear to be affected (29 ± 1.3 and 27 ± 3.5 mU/mg of protein [$n = 5$], respectively). Therefore, Vanin-1 is a modulator of the GSH pool, acting through the γGCS activity. We calculated the GSH/GSSG ratio to evaluate the hepatic redox status in the two genotypes. This ratio was significantly lower in WT controls (≈8.62) than in Vanin-1$^{-/-}$ mice (≈21.02), indicating a more reducing environment in the livers of Vanin-1$^{-/-}$ mice. To better correlate the GSH stores in the liver with Vanin-1$^{-/-}$ protection, we monitored the levels of GSH and GSSG for 2, 4, and 8 days in radiation-treated mice (Fig. 6D). Ionizing radiation led to a dramatic consumption of the endogenous GSH on day 4 in WT mice but a lower consumption in Vanin-1$^{-/-}$ mice. At this time, WT animals began to die, and these values probably explained the difference in the survival curves between the two genotypes (Fig. 6B).

Thereafter, GSH replenishment occurred in animals that survived until day 8. This refill was more marked in Vanin-1$^{-/-}$ mice but was limited when they were treated with cystamine.

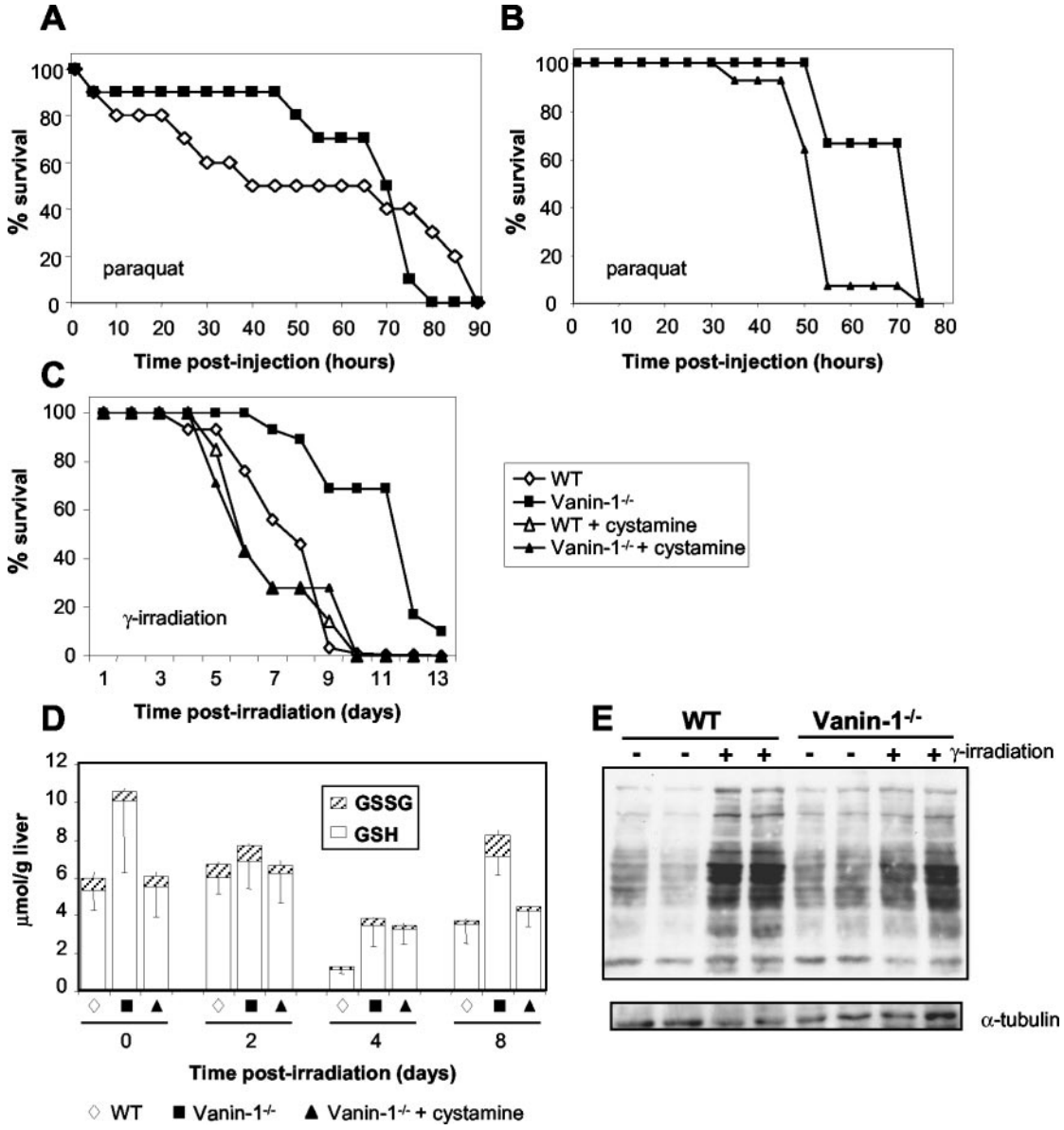

FIG. 6. Vanin-1$^{-/-}$ mice display resistance to systemic oxidative stress caused by paraquat administration or a lethal dose of γ-irradiation. (A and B) Mice were subjected to intraperitoneal administration of paraquat (70 μg/g of body weight). Comparison of the survival between WT and Vanin-1$^{-/-}$ mice ($n = 10$) (A) and comparison of the survival between nontreated ($n = 9$) and cysteamine-treated ($n = 14$) Vanin-1$^{-/-}$ mice in an independent experiment (B) are shown. Intraperitoneal injections of cystamine were done daily (120 mg/kg of body weight). (C) Cohorts of WT ($n = 30$), Vanin-1$^{-/-}$ ($n = 29$), and cysteamine-treated Vanin-1$^{-/-}$ ($n = 7$) female mice were exposed to 10 Gy of γ-irradiation. Survival was plotted in as a percentage of the total. (D) Kinetic analysis of the GSH and GSSG levels in the livers of irradiated mice (10 Gy). Data are expressed in micromoles per gram of liver, and measurements were made on five or six mice. Importantly, for days 4 and 8 postirradiation, values correspond to dosages used on surviving animals. (E) Comparison of oxidized protein levels among liver lysates from WT or Vanin-1$^{-/-}$ mice under normal or postirradiation (4 days, 10 Gy) conditions by detection of protein carbonyl groups (OxyBlot; Oxis). Secondary blotting using antiserum against α-tubulin was performed to verify protein loading (bottom panel). Results are presented for two animals for each condition; this was repeated with two others, giving the same results.

Thus, the resistance of Vanin-1$^{-/-}$ mice to systemic oxidative stress probably relies on their high level of GSH in tissue. In support of this, we found a significant lower ROS concentration in red blood cells of Vanin-1$^{-/-}$ mice compared to WT mice as measured by DCF fluorescence (mean florescence intensity = 51.5 ± 2.5 and 101 ± 20.2 for Vanin-1$^{-/-}$ and WT mice, respectively). We further determined the protein carbonyl contents in the liver as an indicator of the ROS-induced oxidative damage to proteins and found higher levels of oxidized proteins in livers of WT than of Vanin-1$^{-/-}$ mice after irradiation (Fig. 6E). Thus, the absence of Vanin-1 is associated with higher endogenous GSH levels, limiting ROS accumulation and tissue oxidative damage.

Using the Nernst equation, $E_{hc} = -240-(59.1/2) \log ([GSH]^2/[GSSG])$, we evaluated the half-cell reduction potential (E_{hc}) in WT and Vanin-1$^{-/-}$ mouse livers as an indicator

of the biological status of cells (38) and found that it was −289 and −309 mV in WT and Vanin-1$^{-/-}$ mice, respectively. The more positive E_{hc} (GSH) becomes, the larger the number of cells that lose their ability to control their redox environment and then die (38). At 4 days after irradiation, while the WT mice began to die, these values increased in a similar way (+ 20 to 25 mV) in WT (≃−269 mV) and Vanin-1$^{-/-}$ (≃−285 mV) mice. However, Vanin-1$^{-/-}$ mouse tissue kept a reduction potential comparable to the value measured in WT mice under physiological conditions. Thus, the redox environment of a tissue is modulated by the presence of Vanin-1.

DISCUSSION

The mouse epithelial Vanin-1 molecule encodes a pantetheinase activity which releases cysteamine in tissues (34). The initial characterization of Vanin-1 suggested an involvement in the process of thymic reconstitution following irradiation (3). Using Vanin-1$^{-/-}$ mice, our results indicate that Vanin-1 acts as a regulator of the tissue response to oxidative stress by modulation of the GSH store.

The work presented here indicates that in the absence of Vanin-1, thymic reconstitution following a sublethal dose of γ-irradiation is accelerated two- to threefold. This accelerated reconstitution rate could not be accounted for by a reduction in thymocyte apoptosis induced by irradiation and/or alterations in thymocyte differentiation, which did not differ between WT and Vanin-1$^{-/-}$ mice (data not shown). Here, Vanin-1 expression in thymus is shown to be restricted to a subset of EpCAM^{+} CD11c^{-} medullary TECs and transiently up-regulated by whole-body irradiation. This was confirmed in vivo in other tissues such as the liver and kidney and in vitro using other cellular stress inductors such as H_2O_2 and *t*-BHQ. In conclusion, all experiments performed document a two- to fourfold increase of Vanin-1 transcription in tissue on stress induction. Recently, a 2.7-fold transcriptional up-regulation of Vanin-1 was found in renal ischemia-reperfusion in rats (48), a tissue injury model caused mainly by oxidative stress (19, 26). As expected, we demonstrated that the transcriptional activation is associated with enhancement of the cell surface expression of the Vanin-1 protein.

We then identified two functional ARE-like elements within the Vanin-1 promoter. AREs are known regulators of stress-related genes (21). The Vanin-1-proximal ARE-L1 overlaps a CRCGTGRY USF1 binding site, forming a composite USF-ARE sequence that is also found in the proximal promoter of the MT-1 gene, where it is required for basal transcription and induction by H_2O_2 and *t*-BHQ (1). Moreover, the MT-1 binding site was capable of competing with ARE-L1 in the EMSA (Fig. 4D). EMSAs identified AP-1 binding activity to the ARE-L1 site. Consistent with data reported here, AP-1 binding to mouse MT-1 and others AREs is redox sensitive and leads to the coordinate expression of protective antioxidant and proinflammatory genes (7, 35). More puzzling is the binding of SP-1 to ARE-L2, since no bona fide SP-1 consensus site (GGGCGGG) is included in the ARE-L2 sequence. However, although it is generally accepted that SP-1 regulates the expression of housekeeping genes, recent studies have shown that SP-1 binding is increased by stress and confers resistance to oxidative stress (37, 39).

Interestingly, after the first 3 days postirradiation, the early enhancement of the Vanin gene transcription was followed by down-regulation. The distal ARE-L2 site seems to contribute to a negative regulation process, since its mutation led to enhanced expression of the reporter gene. A similar situation has been described for the γGCSh gene promoter, where transforming growth factor β1 (TGF-β1) enhanced the expression of a short γGCSh reporter but down-regulated the expression of a longer construct containing the ARE4 site, which plays a role in the inhibition of γGCSh by TGF-β1 (20). In addition, the Vanin-1 promoter contains E-box motifs (not shown) involved in gene regression mediated by the anti-inflammatory cytokine TGF-β (25). The massive thymocyte apoptosis that occurs after irradiation is known to release mitochondrial TGF-β into the surrounding milieu (5) and could contribute to this down-regulation.

Irradiation induces apoptosis and provokes the recruitment of phagocytes, which scavenge the damaged cells and produce proinflammatory mediators (27, 44). As already described for irradiated rat thymus, early induction of IL-1β and IL-6 expression was associated with myeloid cell recruitment and activation (31). In Vanin-1$^{-/-}$ mice, the higher reconstitution rate following irradiation is correlated with reduced inflammation. In the small intestine, where Vanin-1 is highly expressed by enterocytes (30), fewer apoptotic cells were present in the mucosa of the ileum of a Vanin-1$^{-/-}$ mouse compared to a WT control following irradiation. This argues for a contribution of Vanin-1 to the radiation-induced apoptotic response of intestinal cells. Finally, exposure to systemic oxidative stress created by poisoning with paraquat or a lethal dose of γ-irradiation revealed a significant delayed mortality of the Vanin-1$^{-/-}$ mice. Importantly, in all in vivo models, administration of cysteamine to these mice abrogated their protective phenotype. All this indicates that lack of Vanin-1 up-regulates tissue resistance to oxidative stress and that this is due mainly to the absence of cysteamine in tissue.

Vanin-3 is expressed predominantly by myeloid cells but also by a few epithelial cells in some organs (e.g., thymus and liver) (29). We report the inducible expression of Vanin-3 (two- to sixfold) on stress induction, but the two ARE elements found in the 5′-flanking region of the Vanin-3 gene (positions −1226 and −2813) were not sufficient to significantly respond to the *t*-BHQ treatment in a luciferase assay (data not shown), suggesting the existence of alternative mechanisms in response to stress stimuli. All results document a different kinetic in the transcriptional activation of Vanin-3 compared to Vanin-1. Surprisingly, we observed the up-regulation of Vanin-3 in Vanin-1$^{-/-}$ tissues even though we did not detect cysteamine in the livers of Vanin-1$^{-/-}$ mice (34), suggesting that the functions of the two mouse Vanin molecules might not completely overlap. Further studies are in progress to investigate the role of Vanin-3.

One major finding here is that Vanin-1$^{-/-}$ mice show a higher γGCS activity and consequently augmented GSH stores in tissues. This elevated GSH level is correlated with lower ROS concentrations and oxidative damage in tissue and is linked to the survival of animals exposed to stress. In agreement, injection of GSH-ester in mice leads to an increase in tissue GSH levels and is effective for the prevention of oxidative stress and for radioprotection (24, 46).

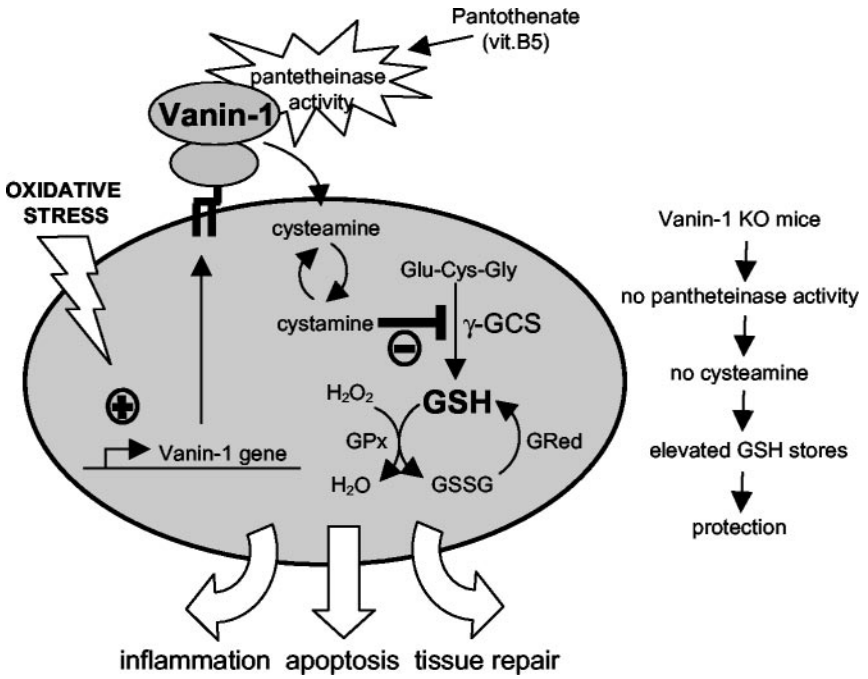

FIG. 7. Vanin-1 as a sensor of oxidative stress. The Vanin-1 gene is regulated on stress induction, and the pantetheinase activity of the cell surface molecule provides tissue with cysteamine through the metabolism of pantothenate (vitamin B_5). One major effect is the γGCS-mediated regulation of the endogenous GSH pool, influencing the redox status and therefore the cell fate in response to oxidative stress injury.

Since GSH is the most abundant redox buffer in cell, measurements of total GSH and GSSG levels have often been used to estimate the redox environment of a cell (38). Variations in the reduction potential of a tissue can regulate the redox-sensitive signaling pathways involved in inflammation and the protective antioxidant response (14, 15, 35, 41). Therefore, this might explain the better tolerance of the Vanin-1$^{-/-}$ mice, where the half-cell reduction potential always remained less positive than the one calculated for WT mice under both normal and stress-related conditions. In normal mice, the stress-induced biphasic expression of Vanin-1 should finely tune the redox environment and thus change an early inflammatory process into a late tissue repair process. Furthermore, this decision is taken at the level of the Vanin-1-expressing epithelial cells and modulates downstream tissue defenses against aggression.

These results for oxidative stress responses generalize recent findings based on experiments on infection or drug-induced intestinal inflammatory models, where we showed that Vanin-1$^{-/-}$ mice display down-regulated inflammation (30). Therefore, we consider Vanin-1 to be a novel tissue sensor for oxidative stress, which couples the vitamin B_5 metabolism to the GSH redox system, and finally, Vanin-1 regulates cell fate after stress injury, in part through the cysteamine-mediated modulation of the γGCS activity (Fig. 7). Importantly, in contrast to the classical use of cysteamine as a radiation-protecting agent, this study shows that the absence of Vanin-1 and the lack of cysteamine in tissue confers to an animal a better resistance to oxidative stress and challenges the use of cysteamine as a radiation protecting agent. Consequently, Vanin/pantetheinase inhibitors will be useful for preventive or therapeutic treatments of irradiation and pro-oxidant inducers.

ACKNOWLEDGMENTS

We thank Rodolphe Guinamard and Johnathan Ewbank and Jeffrey S. Friedman for helpful discussions; Marc Bajenoff, Marc Barad, Mathieu Fallet, and Nicole Brun for assistance in confocal microscopy and flow cytofluorometric analysis; and Marie Françoise Luciani for fluorescence microscopy.

This study was supported by institutional grants from INSERM and CNRS as well as charitable funds from the Association pour la Recherche contre le Cancer (ARC 5945) and Association F. Aupetit (AFA). F. Martin, C. Berruyer, and F. Malergue were recipients of a grant from the Ministère de l'Education Nationale, de la recherche et de la Technologie and of the Ligue Nationale contre le Cancer (LNCC).

REFERENCES

1. **Andrews, G. K.** 2000. Regulation of metallothionein gene expression by oxidative stress and metal ions. Biochem. Pharmacol. **59:**95–104.
2. **Arudchelvan, Y., N. Tokuda, M. Tamechika, Y. H. Wang, N. Mizutani, T. Sawada, K. Yamaguchi, T. Fukumoto, and F. Shinozaki.** 2000. Semiquantitative morphological analysis of stromal cells in the irradiated and recovering rat thymus. Arch. Histol. Cytol. **63:**147–157.
3. **Aurrand-Lions, M., F. Galland, H. Bazin, V. Zakharyev, B. A. Imhof, and P. Naquet.** 1996. Vanin-1, a novel GPI-linked perivascular molecule involved in thymus homing. Immunity **5:**391–405.
4. **Chanas, S. A., Q. Jiang, M. McMahon, G. K. McWalter, L. I. McLellan, C. R. Elcombe, C. J. Henderson, C. R. Wolf, G. J. Moffat, K. Itoh, M. Yamamoto, and J. D. Hayes.** 2002. Loss of the Nrf2 transcription factor causes a marked reduction in constitutive and inducible expression of the glutathione *S*-transferase Gsta1, Gsta2, Gstm1, Gstm2, Gstm3 and Gstm4 genes in the livers of male and female mice. Biochem. J. **365:**405–416.
5. **Chen, W., M. E. Frank, W. Jin, and S. M. Wahl.** 2001. TGF-beta released by apoptotic T cells contributes to an immunosuppressive milieu. Immunity **14:**715–725.
6. **Costello, R., C. Lipcey, M. Algarte, C. Cerdan, P. A. Baeuerle, D. Olive, and J. Imbert.** 1993. Activation of primary human T-lymphocytes through CD2 plus CD28 adhesion molecules induces long-term nuclear expression of NF-kappa B. Cell Growth Differ. **4:**329–339.
7. **Dalton, T. P., Q. Li, D. Bittel, L. Liang, and G. K. Andrews.** 1996. Oxidative stress activates metal-responsive transcription factor-1 binding activity. Occupancy in vivo of metal response elements in the metallothionein-I gene promoter. J. Biol. Chem. **271:**26233–26241.

8. **Di Ilio, C., G. Polidoro, A. Arduini, A. Muccini, and G. Federici.** 1983. Glutathione peroxidase, glutathione reductase, glutathione *S*-transferase, and gamma- glutamyltranspeptidase activities in the human early pregnancy placenta. Biochem. Med. **29:**143–148.
9. **Dupre, S., M. T. Graziani, M. A. Rosei, A. Fabi, and E. Del Grosso.** 1970. The enzymatic breakdown of pantethine to pantothenic acid and cystamine. Eur. J. Biochem. **16:**571–578.
10. **Galland, F., F. Malergue, H. Bazin, M. G. Mattei, M. Aurrand-Lions, C. Theillet, and P. Naquet.** 1998. Two human genes related to murine vanin-1 are located on the long arm of human chromosome 6. Genomics **53:**203–213.
11. **Granjeaud, S., P. Naquet, and F. Galland.** 1999. An ESTs description of the new vanin gene family conserved from fly to human. Immunogenetics **49:** 964–972.
12. **Griffith, O. W., A. Larsson, and A. Meister.** 1977. Inhibition of gamma-glutamylcysteine synthetase by cystamine: an approach to a therapy of 5-oxoprolinuria (pyroglutamic aciduria). Biochem. Biophys. Res. Commun. **79:** 919–925.
13. **Habig, W. H., and W. B. Jakoby.** 1981. Assays for differentiation of glutathione *S*- transferases. Methods Enzymol **77:**398–405.
14. **Haddad, J. J.** 2000. Glutathione depletion is associated with augmenting a proinflammatory signal: evidence for an antioxidant/pro-oxidant mechanism regulating cytokines in the alveolar epithelium. Cytokines Cell. Mol. Ther. **6:**177–187.
15. **Haddad, J. J.** 2002. The involvement of L-gamma-glutamyl-L-cysteinyl-glycine (glutathione/GSH) in the mechanism of redox signaling mediating MAPK(p38)- dependent regulation of pro-inflammatory cytokine production. Biochem. Pharmacol. **63:**305–320.
16. **Haley, T. J.** 1979. Review of the toxicology of paraquat (1,1′-dimethyl-4,4′-bipyridinium chloride). Clin. Toxicol. **14:**1–46.
17. **Hayes, J. D., and L. I. McLellan.** 1999. Glutathione and glutathione-dependent enzymes represent a co-ordinately regulated defence against oxidative stress. Free Radic. Res. **31:**273–300.
18. **Heid, C. A., J. Stevens, K. J. Livak, and P. M. Williams.** 1996. Real time quantitative PCR. Genome Res. **6:**986–994.
19. **Horikawa, S., R. Yoneya, Y. Nagashima, K. Hagiwara, and H. Ozasa.** 2002. Prior induction of heme oxygenase-1 with glutathione depletor ameliorates the renal ischemia and reperfusion injury in the rat. FEBS Lett. **510:**221–224.
20. **Jardine, H., W. MacNee, K. Donaldson, and I. Rahman.** 2002. Molecular mechanism of transforming growth factor (TGF)-beta1-induced glutathione depletionin alveolar epithelial cells. Involvement of AP-1/ARE and Fra-1. J. Biol. Chem. **277:**21158–21166.
21. **Jeyapaul, J., and A. K. Jaiswal.** 2000. Nrf2 and c-Jun regulation of antioxidant response element (ARE)-mediated expression and induction of gamma- glutamylcysteine synthetase heavy subunit gene. Biochem. Pharmacol. **59:**1433–1439.
22. **Klug, D. B., C. Carter, I. B. Gimenez-Conti, and E. R. Richie.** 2002. Cutting edge: thymocyte-independent and thymocyte-dependent phases of epithelial patterning in the fetal thymus. J. Immunol. **169:**2842–2845.
23. **Lebo, R. V., and N. M. Kredich.** 1978. Inactivation of human gamma- glutamylcysteine synthetase by cystamine. Demonstration and quantification of enzyme-ligand complexes. J. Biol. Chem. **253:**2615–2623.
24. **Levy, E. J., M. E. Anderson, and A. Meister.** 1993. Transport of glutathione diethyl ester into human cells. Proc. Natl. Acad. Sci. USA **90:**9171–9175.
25. **Liu, D., B. L. Black, and R. Derynck.** 2001. TGF-beta inhibits muscle differentiation through functional repression of myogenic transcription factors by Smad3. Genes Dev. **15:**2950–2966.
26. **Lloberas, N., J. Torras, I. Herrero-Fresneda, J. M. Cruzado, M. Riera, I. Hurtado, and J. M. Grinyo.** 2002. Postischemic renal oxidative stress induces inflammatory response through PAF and oxidized phospholipids. Prevention by antioxidant treatment. FASEB J. **16:**908–910.
27. **Lorimore, S. A., P. J. Coates, G. E. Scobie, G. Milne, and E. G. Wright.** 2001. Inflammatory-type responses after exposure to ionizing radiation in vivo: a mechanism for radiation-induced bystander effects? Oncogene **20:**7085–7095.
28. **Maras, B., D. Barra, S. Dupre, and G. Pitari.** 1999. Is pantetheinase the actual identity of mouse and human vanin-1 proteins? FEBS Lett. **461:**149–152.
29. **Martin, F., F. Malergue, G. Pitari, J. M. Philippe, S. Philips, C. Chabret, S. Granjeaud, M. G. Mattei, A. J. Mungall, P. Naquet, and F. Galland.** 2001. Vanin genes are clustered (human 6q22–24 and mouse 10A2B1) and encode isoforms of pantetheinase ectoenzymes. Immunogenetics **53:**296–306.
30. **Martin, F., M. F. Penet, F. Malergue, H. Lepidi, A. Dessein, F. Galland, M. de Reggi, P. Naquet, and B. Gharib.** 2004. Vanin-1$^{-/-}$ mice show decreased NSAID- and *Schistosoma*-induced intestinal inflammation associated with higher glutathione stores. J. Clin. Investig. **113:**591–597.
31. **Mizutani, N., Y. Fujikura, Y. H. Wang, M. Tamechika, N. Tokuda, T. Sawada, and T. Fukumoto.** 2002. Inflammatory and anti-inflammatory cytokines regulate the recovery from sublethal X irradiation in rat thymus. Radiat. Res. **157:**281–289.
32. **Mulcahy, R. T., M. A. Wartman, H. H. Bailey, and J. J. Gipp.** 1997. Constitutive and beta-naphthoflavone-induced expression of the human gamma-glutamylcysteine synthetase heavy subunit gene is regulated by a distal antioxidant response element/TRE sequence. J. Biol. Chem. **272:**7445–7454.
33. **Naspetti, M., M. Aurrand-Lions, J. DeKoning, M. Malissen, F. Galland, D. Lo, and P. Naquet.** 1997. Thymocytes and RelB-dependent medullary epithelial cells provide growth- promoting and organization signals, respectively, to thymic medullary stromal cells. Eur. J. Immunol. **27:**1392–1397.
34. **Pitari, G., F. Malergue, F. Martin, J. M. Philippe, M. T. Massucci, C. Chabret, B. Maras, S. Dupre, P. Naquet, and F. Galland.** 2000. Pantetheinase activity ofmembrane-bound vanin-1: lack of free cysteamine in tissues of vanin-1 deficient mice. FEBS Lett. **483:**149–154.
35. **Rahman, I., and W. MacNee.** 2000. Regulation of redox glutathione levels and gene transcription in lung inflammation: therapeutic approaches. Free Radic. Biol. Med. **28:**1405–1420.
36. **Rushmore, T. H., M. R. Morton, and C. B. Pickett.** 1991. The antioxidant responsive element. Activation by oxidative stress and identification of the DNA consensus sequence required for functional activity. J. Biol. Chem. **266:**11632–11639.
37. **Ryu, H., J. Lee, B. A. Olofsson, A. Mwidau, A. Deodeoglu, M. Escudero, E. Flemington, J. Azizkhan-Clifford, R. J. Ferrante, and R. R. Ratan.** 2003. Histone deacetylase inhibitors prevent oxidative neuronal death independent of expanded polyglutamine repeats via an Sp1-dependent pathway. Proc. Natl. Acad. Sci. USA **100:**4281–4286.
38. **Schafer, F. Q., and G. R. Buettner.** 2001. Redox environment of the cell as viewed through the redox state of the glutathione disulfide/glutathione couple. Free Radic. Biol. Med. **30:**1191–1212.
39. **Schafer, G., T. Cramer, G. Suske, W. Kemmner, B. Wiedenmann, and M. Hocker.** 2003. Oxidative stress regulates vascular endothelial growth factor-A gene transcription through Sp1- and Sp3-dependent activation of two proximal GC-rich promoter elements. J. Biol. Chem. **278:**8190–8198.
40. **Seelig, G. F., and A. Meister.** 1985. Glutathione biosynthesis; gamma- glutamylcysteine synthetase from rat kidney. Methods Enzymol **113:**379–390.
41. **Soberman, R. J.** 2003. The expanding network of redox signaling: new observations, complexities, and perspectives. J. Clin. Investig. **111:**571–574.
42. **Somosy, Z., G. Horvath, A. Telbisz, G. Rez, and Z. Palfia.** 2002. Morphological aspects of ionizing radiation response of small intestine. Micron **33:**167–178.
43. **Takada, A., Y. Takada, C. C. Huang, and J. L. Ambrus.** 1969. Biphasic pattern of thymus regeneration after whole-body irradiation. J. Exp. Med. **129:**445–457.
44. **Uchimura, E., N. Watanabe, O. Niwa, M. Muto, and Y. Kobayashi.** 2000. Transient infiltration of neutrophils into the thymus in association with apoptosis induced by whole-body X-irradiation. J. Leukoc. Biol. **67:**780–784.
45. **Wasserman, W. W., and W. E. Fahl.** 1997. Functional antioxidant responsive elements. Proc. Natl. Acad. Sci. USA **94:**5361–5366.
46. **Wellner, V. P., M. E. Anderson, R. N. Puri, G. L. Jensen, and A. Meister.** 1984. Radioprotection by glutathione ester: transport of glutathione ester into human lymphoid cells and fibroblasts. Proc. Natl. Acad. Sci. USA **81:**4732–4735.
47. **Wild, A. C., and R. T. Mulcahy.** 2000. Regulation of gamma-glutamylcysteine synthetase subunit gene expression: insights into transcriptional control of antioxidant defenses. Free Radic. Res. **32:**281–301.
48. **Yoshida, T., M. Kurella, F. Beato, H. Min, J. R. Ingelfinger, R. L. Stears, R. D. Swinford, S. R. Gullans, and S. S. Tang.** 2002. Monitoring changes in gene expression in renal ischemia-reperfusion in the rat. Kidney Int. **61:** 1646–1654.